Photochemistry and Photobiology, 2007, 83: 692–697

The Surface Oxidation Potential of Melanosomes Measured by Free Electron Laser-Photoelectron Emission Microscopy

Jacob Garguilo[1], Lian Hong[2], Glenn S. Edwards[3], Robert J. Nemanich[1] and John D. Simon*[2]

[1]Department of Physics, North Carolina State University, Raleigh, NC
[2]Department of Chemistry, Duke University, Durham, NC
[3]Department of Physics and Free Electron Laser Laboratory, Duke University, Durham, NC

Received 11 September 2006; accepted 26 September 2006; published online 28 September 2006; DOI: 10.1562/2006-09-11-RA-1037

ABSTRACT

A technique for measuring the photoionization spectrum and the photoelectron emission threshold of a microscopic structured material is presented. The theoretical underpinning of the experiment and the accuracy of the measurements are discussed. The technique is applied to titanium silicide nanostructures and melanosomes isolated from human hair, human and bovine retinal pigment epithelium cells, and the ink sac of *Sepia officinalis*. A common photothreshold of 4.5 ± 0.2 eV is found for this set of melanosomes and is attributed to the photoionization of the eumelanin pigment. The relationship between the photoionization threshold and the electrochemical potential referenced to the normal hydrogen electrode is used to quantify the surface oxidation potential of the melanosome. The developed technique is used to examine the effect of iron chelation on the surface oxidation potential of *Sepia* melanosomes. The surface oxidation potential is insensitive to bound Fe(III) up to saturation, suggesting that the metal is bound to the interior of the granule. This result is discussed in relation to the age-dependent accumulation of iron in human melanosomes in both the eye and brain.

INTRODUCTION

Melanin is found in the skin, hair, eyes, inner ear and brain of the human body. Variations in concentration and distribution of melanin pigments—eumelanin (black) and pheomelanin (red)—account for the color range in human skin, hair and irises. In addition to generating color, a number of biological functions are commonly ascribed to melanins, including photoprotection (1–3), free radical scavenging (4) and the sequestering of transition metal cations (5), such as Fe(III), Cu(II) and Zn(II).

Melanin is synthesized in cellular organelles called melanosomes. The details of this process are not understood; however, the initial steps involve the enzymatic oxidation of tyrosine (6). In the case of eumelanin, the oxidized products 5, 6-dihydroxyindole (DHI) and 5,6-dihydroxyindole-2-carboxylic acid (DHICA) are hypothesized to be the major molecular building blocks that oligomerize to form the pigment. Transmission electron micrographs of black melanosomes in the early stages of pigmentation reveal the presence of a scaffold, presumed to be a proteinaceous material, within the organelle (7). Pigment deposits appear along this scaffold and expand to fill the organelle. Atomic force microscopy (AFM) studies reveal substructure, suggesting that melanosomes are comprised of ~30 nm subunits (8–10).

One of the most important topics regarding melanin focuses on the ability of the pigment to both mitigate and cause oxidative stress. The former is considered to be protective; the latter is deleterious to human health. The balance between the oxidative and reductive behavior of the pigment likely plays an important role in modulating stress, most notably in the skin (11), retinal pigment epithelium (RPE) (5,12,13) and *Substantia nigra* (14,15). Small eumelanin oligomers have been identified as the important constituents resulting in photoinduced formation of reactive oxygen species (16) and their aggregation mitigates these processes (17), and so knowledge of the surface oxidation potential would serve as a fundamental starting point for assessing the role of the melanosomes in such processes. Unfortunately, the oxidation potential of human melanins has not been determined.

Photoelectron emission microscopy (PEEM) is a powerful approach for obtaining spatially resolved images of intact biological organelles (18). Images have been reported for viruses (19), eukaryotic cells (20), cultured cancer cells (21) and cytoskeletons (22), although a number of these samples required metal coating to alleviate their low electrical conductivity. There have also been a number of studies detailing the photoemission quantum yields of biological samples (23,24).

Recently, we have exploited the tunability of the Duke OK-4 free electron laser (FEL) to determine the photothresholds of black and red melanosomes isolated from human hair (25). Herein, we focus on the threshold potential of eumelanosomes from a variety of natural sources and examine the theoretical analysis of the data and possible effects of transient heating by the incident FEL beam. The connection between the vacuum threshold potential and the electrochemical potential *versus* NHE is also discussed. The data on melanosomes are then presented and framed in terms of their ability to induce oxidative stress. Specifically, the effect of iron concentration on the oxidation potential is explored.

MATERIALS AND METHODS

Melanosomes. Details of the isolation and characterization of melanosome samples from human hair and eyes, bovine eyes and from the

*Corresponding author email: jsimon@duke.edu (John D. Simon)

ink sac of the *Sepia officinalis* as well as the preparation and characterization of the Fe(III)-loaded *Sepia* granules have been published previously (26–28). After isolation, the melanosome suspension was diluted in Nanopure water and spread over RCA-cleaned silicon wafers (n-type, ⟨100⟩, resistivity 0.05–0.1 Ω cm). The RCA cleaning procedure results in a surface terminated with an ~1 nm thick silicon oxide layer. The films were allowed to dry for no more than 1 h and then placed into the vacuum system. The films of melanosomes were all submonolayer in thickness.

Titanium samples. A section of a silicon wafer (n-type, ⟨111⟩, resistivity 0.8–1.2 Ω cm) was employed as the substrate for the titanium silicide sample. The wafer was cleaned by UV-ozone exposure followed by an HF-based spin etch, and then by *in situ* annealing at 900°C for 10 min (base pressure $\leq 2 \times 10^{-10}$ Torr). About two monolayers of Ti were deposited by electron beam evaporation at a rate of one monolayer per minute onto the clean Si surface at room temperature by electron beam evaporation. The sample was then heated to 1000°C for 10 min to induce $TiSi_2$ island and nanowire formation (29), cooled to room temperature and examined with the forthcoming UV-PEEM procedure.

FEL-PEEM measurements. The PEEM measurements were carried out in an Elmitec UHV photoelectron emission microscope. The field of view of the instrument can be varied between 1.5 and 185 μm with a maximal resolution of < 15 nm and a base pressure of $\leq 2 \times 10^{-10}$ Torr. A high voltage of 20 kV is applied between the anode and the sample surface, with the sample being held negative, in order to accelerate the emitted electrons through the electron optics of the microscope. The distance between the anode and sample surface was typically ~4 mm resulting in an applied field of ~5 V μm^{-1}. Electrons emitted from the sample pass through a perforated anode and are imaged with a fluorescent screen. A microchannel plate between the fluorescent screen and electron optics intensifies the image and a CCD camera records the data.

We utilized the spontaneous emission mode of the Duke UV-FEL in the spectral range 206.5–413.5 nm (6.0–3.0 eV), with an energy full width at half-maximum of ~0.1 eV. The specifications of the Duke FEL are described elsewhere (30). The output radiation of the FEL in spontaneous mode at high energies corresponds to the on-axis radiation in the forward light cone for the fundamental harmonic only. At high photon energies (> 4 eV), the higher harmonics do not affect the PEEM images due to almost complete absorption in the air and optics. For energies at or below 4 eV, a cut-off filter was inserted into the beam line (~95% transmission at 4 eV) to negate any harmonic effects for low energies.

Image processing. The PEEM images for each wavelength were recorded with a DVC 1312M digital camera from DVC Company, Inc. (Austin, TX). The camera resolution is 1300 × 1030 pixels × 12 bits. The DVC View program was used to display and save images. We typically imaged assemblies of eumelanosomes at fields of view in the PEEM of 20 μm. The FEL spot size can be described by an elongated oval with axial dimensions of approximately 30 and 100 μm. The FEL focus was optimized for each wavelength.

An image for each wavelength of light, corresponding to a single data point on the photoionization threshold curves, was recorded using the above software and converted to an 8-bit file. An area in each image, corresponding to one or to a few melanosomes, was then selected at each wavelength, and the histogram of the region was copied and pasted into either Excel or Igor software. The size and shape of the selected region were kept constant between wavelength images. The X column of the histogram contains 8-bit-scale gray scale depths, i, in units from 0 to 255, and the Y column contains the number of pixels, $N(i)$, in the histogram, having the given gray scale depth, i. At each wavelength examined, the integrated brightness, S, where

$$S = \sum_i iN(i), \tag{1}$$

was calculated for each fragment. This value is taken to be proportional to the photocurrent collected from the region. The integrated brightness for each emitting portion is affected by several instrument parameters. If these instrumental settings are left unchanged during a wavelength sweep, $S(\lambda)$ changes considerably and suffers from intensity saturation. The ideal shape of the intensity histogram would be a Gaussian distribution centered close to $i = 128$. Intensity histograms partially or completely located at $i = 0$ or $i = 255$ are regarded as black or white saturated, respectively. In these cases, information regarding the brightness of the emitting portion is lost, and the photoelectron current is no longer proportional to S. In order to avoid these artifacts, the software gain of the DVC imaging program was adjusted accordingly. The integrated brightness was then corrected using the equation:

$$\text{gain (db)} = 20 \log_{10} G. \tag{2}$$

On occasion, the available software gain does not provide a broad enough range to limit saturation. In these cases, a single change to the voltage across the microchannel plate was used. To calibrate for this change on S, PEEM images were collected at fixed wavelength and software gains, but with different MCP voltages. The ratio of S between the images provided the needed correction factor. The incident photon flux at each wavelength of the FEL also affects the integrated brightness of the emitting region. The incident power of the spontaneous radiation at the input port of the PEEM depends on the current in the FEL storage ring and any absorption that may occur due to optics in the beam path. Because of the large number of permutations possible, power measurements were recorded for each wavelength at a minimum of five different FEL ring currents. The incident power was then taken from linear extrapolations of the data, and S was normalized to a constant photon flux (photons s^{-1}) for each wavelength. The power as a function of FEL ring current for four wavelengths is displayed in Fig. 1. The linear nature of the power *versus* ring current is evident and was observed at all wavelengths of interest. We could not determine the light fluence directly on the sample within the microscope; therefore, the wavelength-dependent data reveal relative, not absolute, photoionization quantum yields.

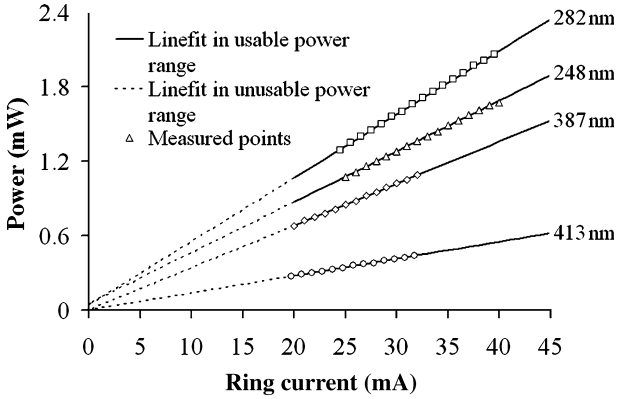

Figure 1. The power incident on the input port of the PEEM is measured as a function of FEL ring current for four representative wavelengths used in this study. The data are well described by a series of linear fits; a single set of parameters is incapable of fitting the data for all excitation energies because of the wavelength-dependent absorption of optics in the beam's path. All images were recorded between 20 and 45 mA ring current and the integrated brightness was normalized to a constant photon flux.

RESULTS AND DISCUSSION

Modeling of the wavelength-dependent PEEM emission

In 1931, Fowler (31) reported an expression for the photoelectric current in the vicinity of the threshold for emission as a function of temperature and frequency of incident radiation. Photoelectric emission data for gold, silver, tin, potassium and tantalum were analyzed based on this model, and the measured values of photocurrent as a function of temperature and incident light displayed excellent agreement to the theoretical fit. Dubridge (32), in 1933, extended the theory presented by

Fowler to account for the energy distribution of the emitted electrons. These papers, taken together, form the basis for what is known as the Fowler–Dubridge theory of photoemission. The experimental data herein were fit using Fowler's first analysis of observation equations. In this treatment, the photocurrent, which we have taken to be proportional to the integrated brightness of the region under analysis, is described by

$$I(\chi_0 - h\nu)^{1/2}/T^2 = Af([h\nu - \chi]/kT), \tag{3}$$

where A is a scaling constant independent of ν and T. In the above equation, $f(u)$ is a term by term integration of the number of available electrons in a certain energy range described by Fowler and is given by

$$f(u) = e^u - e^{2u}/4 + e^{3u}/9 - \cdots \qquad (u \leq 0), \tag{4}$$

$$f(u) = \pi^2/6 + u^2/2 - (e^{-u} - e^{-2u}/4 + e^{-3u}/9 - \cdots) \quad (u \geq 0). \tag{5}$$

The values of the scaling constant, A, and the photothreshold, χ, can be determined by curve fitting software using an iterative Levenberg–Marquardt algorithm that minimizes the chi-square value.

Modeling of the heating due to FEL excitation

The above analysis requires knowledge of the temperature of the sample. In fitting the experimental data to the Fowler equation, this value is taken to be that of the temperature of the substrate in the vacuum chamber. However, the incident light penetrates through the sample and thereby exceeds the escape depth of electrons. Thus, photoionization occurs within the materials, and for the electrons that do not escape, this energy is released through the emission of lattice phonons. This process will result in a temperature increase in the sample. It is important to determine the magnitude of the change relative to the ambient temperature of the sample. The spontaneous emission of the Duke-FEL is well modeled by a train of square-wave pulses. Each train consists of 10 pulses with constant peak power, P, with pulse duration of Δt and a spacing between pulses of T_p. The train has a repetition period of T_t. Following the work by Liau *et al.* (33), the temperature profile of the sample is given by

$$T(z,t) = \int_0^t (1/\rho s)\{\exp(-z^2/4D_h[t-t'])/(\pi D_h[t-t'])^{1/2}\} P(t')\, dt' + T_r, \tag{6}$$

where t is the time, z is the depth into the sample, T_r is room temperature and ρ, s, and D_h are mass density, specific heat and thermal diffusivity of the sample, respectively.

Taking $z = 0$, Eq. (1) yields

$$T(0,t) = T_m(t/\Delta t)^{1/2} + T_r, \tag{7}$$

with T_m, the maximum temperature rise, being given by

$$T_m = (2/\pi^{1/2})\{P\Delta t/(\rho s[D_h \Delta t]^{1/2})\}. \tag{8}$$

Taking the duty cycle of each pulse in the train to be 5×10^{-2} and the duty cycle of the train to be 2×10^{-1}, the peak power of a single pulse is approximately 100 mW. The FEL irradiation, focused to a diameter of 100 μm, is incident on the surface of the sample at an angle of approximately 10° and illuminates an ellipsoidal area. Taking this into consideration and assuming that the entire pulse is delivered to and absorbed by the melanosome, the corresponding maximum temperature rise per peak is 0.012 K. If there is no cooling between pulses in the train, the maximum temperature rise per train is 0.12 K. The time between pulses is approximately 300 ns, which is sufficient for complete cooling, meaning this value represents an overestimate of the ambient rise in sample temperature during the experimental run and the effects of transient heating are negligible. Previous modeling of high-powered infrared pulses delivered by the FEL to alternating layers of protein and saline indicated the possibility of ablation due to heating (34). However, the experimental details presented here are significantly different from the previous study; no rise in temperature was detected at the sample surface during our experiments.

FEL-PEEM results of black pigments

Thin Ti films and $TiSi_2$ represent control measurements for our UV-FEL-PEEM analysis because the work function for the bulk materials has been determined by established methodologies to be 4.33 and 4.53 ± 0.03 eV (35), respectively. We have previously reported the UV-FEL-PEEM results from Ti films, and found a threshold potential of 4.5 ± 0.2 eV (36), in good agreement with the reported work function of 4.33 eV.

The topographic features of the melanosome samples could give rise to "edge effects" that may affect the measured photothreshold values. To address this point, we have examined the threshold potentials of nanostructures of $TiSi_2$. The $TiSi_2$ islands typically have diameters between 200 and 600 nm and are assumed to be approximately hemispherical in shape. Figure 2 presents a PEEM image of the $TiSi_2$ islands and nanowires obtained at photon energies of 5.0 eV. The wavelength-dependent intensity data for the central nanowire in the image is also shown. The data are well described by Eqs. (3)–(5), revealing a photothreshold of 4.7 ± 0.2 eV, also in good agreement with the reported work function. Therefore, we conclude that the topographic features of $TiSi_2$ nanostructures do not result in a significant deviation of the measured photothreshold.

FEL-PEEM images were collected for melanosomes isolated from black human hair, the ink sacs of *Sepia*, bovine RPE

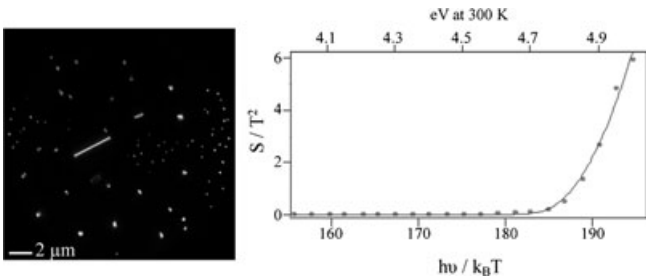

Figure 2. A PEEM image of $TiSi_2$ islands and nanowires taken at 248 nm illumination is presented on the left. The central nanowire's wavelength-dependent emission is shown on the right (points) and the fit to the data (line) reveals a photothreshold of 4.7 ± 0.2 eV which is in reasonable agreement with the reported value of 4.53 ± 0.03 eV. Analysis of islands resulted in an identical photothreshold value.

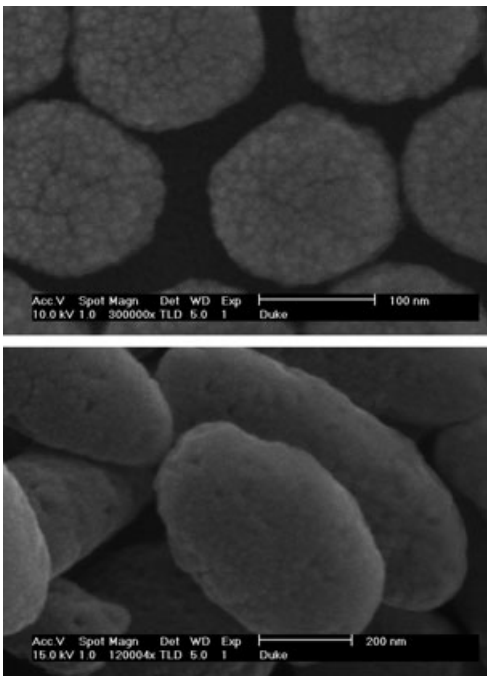

Figure 3. SEM images of melanin granules from *Sepia officinalis* (top) and melanosomes isolated from human black hair (bottom).

cells, and human RPE cells. Melanosome samples have more significant topography than the $TiSi_2$ islands, which may affect the vacuum barrier in the photoionization measurements. Figure 3 shows a scanning electron micrograph of melanosomes isolated from the ink sac of *Sepia officinalis* and black human hair. As these images show, *Sepia* melanin granules are about 150 nm of diameter, while black hair melanosomes are mostly ellipsoidal with the long axis about 1 μm. Such ''sharp'' structures could give rise to electric field enhancement, which could affect the measured potential. The most commonly recognized influence of a high electric field is the deflection of the potential barrier and its implications to the phenomenon known as field emission. However, a second consequence of the applied electric field is a lowering of the potential barrier. This is commonly referred to as the Schottky effect. In the case of melanosomes, the field enhancement should be well approximated by a hemispherical geometric object on a plane, which is a system that has been solved exactly and has a field enhancement factor equal to 3 (37). An enhancement of this magnitude would result in a reduction of the vacuum barrier of ~0.13 eV, and while this would be a systematic error in the measurement, it is smaller than the current uncertainty of the measurement, ±0.2 eV. The threshold ionization potentials determined by fitting Eqs. (3)–(5) to the experimental data on a range of black melanosomes show a narrow range: 4.7 (*Sepia*) and 4.4 eV (human and bovine RPE samples and human hair). The dominant species that is photoionized in these samples is eumelanin and all samples studied indicate a surface threshold potential of 4.5 ± 0.2 eV.

FEL-PEEM results of Fe(III) loading on *Sepia*

With increasing age, the photoinduced uptake of oxygen by different age cohorts of human RPE melanosomes shows an increase of the activation of oxygen (38). There are data in support of the conclusion that Fe(III) accumulates in neuronal melanosomes with age (5,39). In addition, RPE melanosomes show an increased blue-light induced emission with age (40), which Schraermeyer and coworkers (41) attribute to oxidation of the pigment. Collectively, these data suggest the age-dependent increase in aerobic photoreactivity reflects a lowering of the surface oxidation potential through either oxidative damage or iron binding. These two mechanisms could also be linked. While Fe(III) is largely unreactive, when reduced to Fe(II), the resulting Fenton chemistry can induce significant oxidative stress in cells. In a recent study on Fe(III) binding by DHI and DHICA, Charkoudian and Franz (42) reported that the oxidation of DHI and especially DHICA are accelerated in the presence of iron. While no oxidation potentials have been reported, these results certainly support the conclusion that upon binding of Fe(III), DHI and DHICA become more reductive. This suggests that the binding of Fe(III) to the surface of the melanosome should affect its oxidation potential, and potentially increase the capacity of the melanosome to induce oxidative stress *in vivo*. What is lacking are experimental data on whether Fe(III) bound to the surface of the melanosome affects the surface oxidation potential.

A previous report from our laboratory presented the analysis of SEM images showing that the diameter and surface characteristics of *Sepia* melanosomes were unaffected by added Fe(III) up to the saturation limit of 86 000 ng mg^{-1} melanin (26). For solution at pH 4, the binding of an individual Fe(III) cation is accompanied by the release of ~3 H^+, suggesting that binding occurs to catechol groups (43). Such binding is consistent with recently reported Raman studies (44). Both the dark- and light-induced aerobic reactivity of *Sepia* granules is enhanced upon saturation with Fe(III) (43). This reactivity is dependent on the buffer used and whether EDTA is present in the solution. And so, it is not clear whether or not the increased reactivity results from a change in surface potential due to Fe(III) binding or changes in the availability of Fe(III) due to experimental conditions.

To address whether Fe(III) binding affects the surface oxidation potential, we determined the threshold photoionization energies for *Sepia* melanosomes with varying levels of Fe(III) up to saturation. The saturation limit corresponds to about one Fe(III) for every four monomeric building blocks in the pigment. The results from EDTA-treated and Fe(III)-saturated *Sepia*, the two limiting cases, are presented in Fig. 4. The threshold photoionization energy for the Fe(III)-saturated sample is within the experimental error of that of the EDTA-treated sample. This result supports the conclusion that the binding of Fe(III) to the melanosome has negligible effect on the surface oxidation potential of the organelle.

The FEL-PEEM results on the iron-loaded samples indicate that the melanosome effectively sequesters Fe(III) up through saturation. If there are changes in the surface structure that accompany iron binding, which would need to be at a level irresolvable by SEM or AFM, such changes do not produce measurable differences in the electrochemical properties. As both RPE melanin and neuromelanin accumulate iron with age, the results on this model system would suggest that such

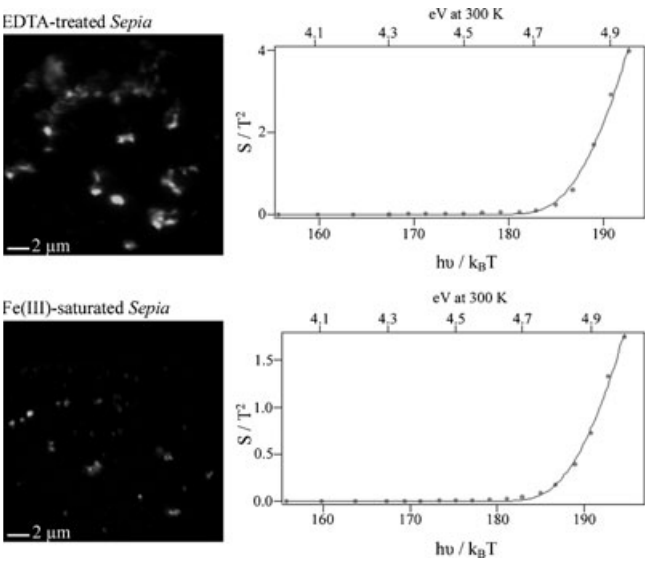

Figure 4. PEEM images of EDTA-treated (upper left) and Fe(III)-saturated (lower left) *Sepia* taken at 248 nm illumination are presented. The wavelength-dependent data for each sample is shown on the right of the respective images. The threshold photoionization energy for both the EDTA-treated sample and the Fe(III)-saturated sample is 4.7 ± 0.2 eV, indicating that the binding of Fe(III) to the melanosome has a negligible effect on the surface oxidation potential of the organelle.

itself does not increase the aerobic reactivity of the pigment. The increased aerobic reactivity of Fe(III)-enriched melanin observed in previous research may be due to the release of free Fe(III) by the pigments into solutions.

CONCLUSION

A procedure for measuring the spatially resolved photothreshold of a heterogeneous sample is established. The technique relies on the imaging capabilities of our PEEM in conjunction with the tunability of the Duke UV-FEL. The data correction and fitting procedure are reviewed and applied to two samples with known photothresholds, thin titanium films and nanostructured $TiSi_2$. The data acquired from these samples are well described by the fitting procedure and the measured photothreshold agrees with reported values, within the error of the measurement. The technique is applied to melanosomes isolated from human hair, human and bovine RPE cells and the ink sac of the *Sepia officinalis* and a common photothreshold of 4.5 ± 0.2 eV is found. This value is attributed to the photoionization of the eumelanin pigment contained in the samples and the relevance to oxidative stress is discussed. To further investigate the role of eumelanin on oxidative stress, the effect of iron loading on the photothreshold of eumelanosomes isolated from *Sepia officinalis* is examined. No measurable difference in the photothreshold is detected from these samples, suggesting that the aerobic reactivity of the pigment is not increased upon accumulation of iron. The increased aerobic reactivity of Fe(III)-enriched pigment observed in previous research may be due to the release of free Fe(III) by the pigments into solutions.

Acknowledgements—The authors would like to acknowledge Dr. Ying Wu for his helpful discussion regarding the FEL. This work is supported by the AFOSR through the MFEL program at Duke University.

REFERENCES

1. Ahene, A. B., S. Saxena and S. Nacht (1994) Photoprotection of solubilized and microdispersed melanin particles. *J. Invest. Dermatol.* **102**, 268.
2. Giacomoni, P. U. (1995) Open questions in photobiology 3. Melanin and photoprotection. *J. Photochem. Photobiol. B, Biol.* **29**, 87–89.
3. Kollias, N., R. M. Sayre, L. Zeise and M. R. Chedekel (1991) Photoprotection by melanin. *J. Photochem. Photobiol. B, Biol.* **9**, 135–160.
4. Bustamante, J., L. Bredeston, G. Malanga and J. Mordoh (1993) Role of melanin as a scavenger of active oxygen species. *Pigment Cell Res.* **6**, 348–353.
5. Sarna, T. (1992) Properties and function of the ocular melanin—A photobiophysical view. *J. Photochem. Photobiol. B, Biol.* **12**, 215–258.
6. Ito, S. (2003) A chemist's view of melanogenesis. *Pigment Cell Res.* **16**, 230–236.
7. Raposo, G., D. Tenza, D. M. Murphy, J. F. Berson and M. S. Marks (2001) Distinct protein sorting and localization to premelanosomes, melanosomes, and lysosomes in pigmented melanocytic cells. *J. Cell Biol.* **152**, 809–823.
8. Liu, Y. and J. D. Simon (2003) Isolation and biophysical studies of natural eumelanins: Applications of imaging technologies and ultrafast spectroscopy. *Pigment Cell Res.* **16**, 606–618.
9. Clancy, C. M. R. and J. D. Simon (2001) Ultrastructural organization of eumelanin from *Sepai officinalis* measured by atomic force microscopy. *Biochemistry* **40**, 13353–13360.
10. Liu, Y., V. R. Kempf, J. B. Nofsinger, E. E. Weinert, M. Rudnicki, K. Wakamatsu, S. Ito and J. D. Simon (2003) Comparison of the structural and physical properties of human eumelanin following enzymatic or acid/base extraction. *Pigment Cell Res.* **16**, 355–365.
11. Vincensi, M. R., M. d'Ischia, A. Napolitano, E. M. Procaccini, G. Riccio, G. Monfrecola, P. Santoianni and G. Prota (1998) Phaeomelanin versus eumelanin as a chemical indicator of ultraviolet sensitivity in fair-skinned subjects at high risk for melanoma: A pilot study. *Melanoma Res.* **8**, 53–58.
12. Boulton, M. (1991) Aging of the retinal-pigment epithelium. *Prog. Retin. Eye Res.* **11**, 125–151.
13. Schraermeyer, U. and K. Heimann (1999) Current understanding on the role of retinal pigment epithelium and its pigmentation. *Pigment Cell Res.* **12**, 219–236.
14. Fornstedt, B., A. Brun, E. Rosengren and A. Carlsson (1989) The apparent autoxidation rate of catechols in dopamine-rich regions of human brains increases with the degree of depigmentation of substantia nigra. *J. Neural Transm. Park. Dis. Dement. Sect.* **1**, 279–295.
15. Zecca, L., F. A. Zucca, H. Wilms and D. Sulzer (2003) Neuromelanin of the substantia nigra: A neuronal black hole with protective and toxic characteristics. *Trends Neurosci.* **26**, 578–580.
16. Nofsinger, J. B., S. E. Forest and J. D. Simon (1999) An explanation for the disparity among the absorption and action spectra of eumelanin. *J. Phys. Chem.* **103**, 11428.
17. Nofsinger, J. B., Y. Liu and J. D. Simon (2002) Aggregation of eumelanin mitigates photogeneration of reactive oxygen species. *Free Radic. Biol. Med.* **32**, 720–730.
18. Edwards, G. S., S. J. Allen, R. F. Haglund, R. J. Nemanich, B. Redlich, J. D. Simon and W.-C. Yang (2005) Applications of free-electron lasers in the biological and material sciences. *Photochem. Photobiol.* **81**, 711–735.
19. Birrell, G. S., D. L. Habliston and O. H. Griffith (1994) Photoelectron imaging of viruses and DNA—Evaluation of substrates by unidirectional low-angle shadowing and photoemission current measurements. *Biophys. J.* **67**, 2041–2047.
20. Griffith, O. H. and G. F. Rempfer (1985) Photoelectron imaging in cell biology. *Annu. Rev. Biophys. Biophys. Chem.* **14**, 113–130.

21. Habliston, D. L., K. K. Hedberg, G. B. Birrell, G. F. Rempfer and O. H. Griffith (1995) Photoelectron imaging of cells—Photoconductivity extends the range of applicability. *Biophys. J.* **69**, 1615–1624.
22. Birrell, G. B., K. K. Hedberg, D. L. Habliston and O. H. Griffith (1991) Biological applications of photoelectron imaging—A practical perspective. *Ultramicroscopy* **36**, 235–251.
23. Griffith, O. H., D. L. Holmbo, D. L. Habliston and K. K. Nadakavukaren (1981) Contrast effects in photoelectron microscopy—UV dose-dependent quantum yields of biological surface components. *Ultramicroscopy* **6**, 149–156.
24. Dam, R. J., K. K. Nadakavukaren and O. H. Griffith (1977) Photoelectron microscopy of cell-surfaces. *J. Microsc.* **111**, 211–217.
25. Samokhvalov, A., L. Hong, Y. Liu, J. Garguilo, R. J. Nemanich, G. S. Edwards and J. D. Simon (2005) Oxidation potentials of human eumelanosomes and pheomelanosomes. *Photochem. Photobiol.* **81**, 145–148.
26. Liu, Y., L. Hong, V. R. Kempf, K. Wakamatsu, S. Ito and J. D. Simon (2004) Ion-exchange and adsorption of Fe(III) by *Sepia* melanin. *Pigment Cell Res.* **17**, 262–269.
27. Liu, Y., L. Hong, K. Wakamatsu, S. Ito, B. B. Adhyaru, C. Y. Cheng, C. R. Bowers and J. D. Simon (2005) Comparison of structural and chemical properties of black and red human hair melanosomes. *Photochem. Photobiol.* **81**, 135–144.
28. Liu, Y., L. Hong, K. Wakamatsu, S. Ito, B. B. Adhyaru, C. Y. Cheng, C. R. Bowers and J. D. Simon (2005) Comparisons of the structural and chemical properties of melanosomes isolated from retinal pigment epithelium, iris and choroid of newborn and mature bovine eyes. *Photochem. Photobiol.* **81**, 510–516.
29. Yang, W.-C., M. Zeman, H. Ade and R. J. Nemanich (2003) Attractive migration and coalescence: A significant process in the coarsening of $TiSi_2$ islands on the Si(111) surface. *Phys. Rev. Lett.* **90**, 136102.
30. Ade, H., W. Yang, S. L. English, J. Hartman, R. F. Davis, R. J. Nemanich, V. N. Litvinenko, I. V. Pinayev, Y. Wu and J. M. J. Madey (1998) A free electron laser-photoemission electron microscope system (FEL-PEEM). *Surf. Rev. Lett.* **5**, 1257–1268.
31. Fowler, R. H. (1931) The analysis of photoelectric sensitivity curves for clean metals at various temperatures. *Phys. Rev.* **38**, 45–56.
32. DuBridge, L. A. (1933) Theory of the energy distribution of photoelectrons. *Phys. Rev.* **43**, 0727–0741.
33. Liau, Z. L., B. Y. Tsaur and J. W. Mayer (1979) Laser annealing for solid-phase thin film reactions. *Appl. Phys. Lett.* **34**, 221–223.
34. Hutson, M. S., S. A. Hauger and G. Edwards (2002) Thermal diffusion and chemical kinetics in laminar biomaterial due to heating by a free-electron laser. *Phys. Rev. E* **65**, 061906.
35. Bucher, E., S. Schulz, M. C. Luxsteiner, P. Munz, U. Gubler and F. Greuter (1986) Work function and barrier heights of transition-metal silicides. *Appl. Phys. A—Mater.* **40**, 71–77.
36. Samokhvalov, A., J. Garguilo, W. C. Yang, G. S. Edwards, R. J. Nemanich and J. D. Simon (2004) Photoionization threshold of eumelanosomes determined using UV free electron laser-photoelectron emission microscopy. *J. Phys. Chem. B* **1081**, 6334–6338.
37. Forbes, R. G., C. J. Edgcombe and U. Valdre (2003) Some comments on models for field enhancement. *Ultramicroscopy* **95**, 57–65.
38. Rozanowsla, M., W. Korytowski, B. Rozanowska, C. Skumatz, M. E. Boulton, J. M. Burke and T. Sarna (2002) Photoreactivity of aged human RPE melanosomes: A comparison with lipofuscin. *Invest. Ophthamol. Vis. Sci.* **43**, 2088–2096.
39. Zecca, L., M. Gallorini, V. Schunemann, A. X. Trautwein, M. Gerlach, P. Riederer, P. Vezzoni and D. Tampellini (2001) Iron, neuromelanin and ferritin content in the substantia nigra of normal subjects at different ages: Consequences for iron storage and neurodegenerative processes. *J. Neurochem.* **76**, 1766–1773.
40. Sarna, T., J. M. Burke, W. Korytowski, M. Rozanowska, C. M. B. Skumatz, A. Zareba and M. Zareba (2003) Loss of melanin from human RPE with aging: Possible role of melanin photooxidation. *Exp. Eye Res.* **76**, 89–98.
41. Kayatz, P., G. Thumann, T. T. Lutherm, J. F. Jordan, K. U. Bartz-Schmidt, P. J. Esser and U. Schraermeyer (2001) Oxidation causes melanin fluorescence. *Invest. Ophthalmol. Vis. Sci.* **42**, 241–246.
42. Charkoudian, L. K. and K. J. Franz (2006) Fe(III)-coordination properties of neuromelanin components: 5,6-Dihydroxyindole and 5,6-dihydroxyindole-2-carboxylic acid. *Inorg. Chem.* **45**, 3657–3664.
43. Hong, L., Y. Liu and J. D. Simon (2004) Binding of metal ions to melanin and its effects on aerobic reactivity. *Photochem. Photobiol.* **80**, 477–481.
44. Samokhvalov, A., Y. Liu and J. D. Simon (2004) Characterization of the Fe(III) binding site in *Sepia* eumelanin by resonance Raman confocal microspectroscopy. *Photochem. Photobiol.* **80**, 84–88.